Study of the decay of hot nuclei formed in ^{139}La-induced reactions at $E/A = 45$ MeV by a hybrid dynamical-statistical calculation

B. Libby* and A. C. Mignerey
Department of Chemistry, University of Maryland, College Park, Maryland 20742

N. Colonna,† P. Roussel-Chomaz,‡ G. J. Wozniak, and L. G. Moretto
Nuclear Science Division, Lawrence Berkeley Laboratory, Berkeley, California 94720
(Received 12 June 1995)

The reactions ^{139}La + ^{27}Al and ^{139}La + ^{65}Cu at $E/A = 45$ MeV have been modeled by combining a Boltzmann-Nordheim-Vlasov dynamical model calculation with a statistical sequential binary decay model code. For the reaction ^{139}La + ^{27}Al, the major features of the experimental data are adequately described by the model calculations. These features include the inclusive fragment cross sections and the total charge and source velocity distributions of multiple fragment events. Other finer features, such as charge-Dalitz plots and the branching ratios between events of different multiplicity, are not reproduced by the calculation. The failure of the calculations is even greater for the reaction ^{139}La + ^{65}Cu, in which only the source velocity distributions of multiple fragment events are reproduced. Because the source velocity can be a measure of how much of the target is incorporated into the projectile in inverse kinematics reactions, this suggests that the earliest stages of the reaction, described by the dynamical calculation, are adequately characterized by the model. It is the later stages of the reaction, when fragments are emitted, where the model calculation appears to fail. However, there are some indications that statistical decay in the reaction ^{139}La + ^{65}Cu has occurred, whether by sequential binary decays or some type of prompt multifragmentation. [S0556-2813(96)04206-9]

PACS number(s): 25.70.Pq, 24.10.−i

I. INTRODUCTION

In recent years, the emission of complex fragments ($Z>2$), also known as intermediate mass fragments (IMF's), in intermediate energy heavy-ion reactions has been extensively studied, both experimentally [1–16] and theoretically [17–24]. The emission of several (more than two) complex fragments has been loosely dubbed ''multifragmentation.'' However, many fragment final states can arise both by sequential emission [1–4] and by simultaneous breakup of a highly excited nucleus [18]. Differentiating between these competing mechanisms experimentally can be difficult, which leads to the use of decay simulations [3] and reaction model calculations [25–28] to help interpret the experimental data. Additionally, the same data can be interpreted by calculations from competing reaction models [1,5,20], further complicating the picture. Aside from differentiating between sequential and simultaneous decay mechanisms, research has concentrated on the roles of dynamics and statistics in the mechanism of complex fragment emission, and the possible interplay between the two [2,12,25–28].

In order to explore the competition between sequential binary decay and ''true'' prompt multifragmentation, and the interplay between statistics and dynamics, it is necessary to model reactions in such a way that both dynamical effects and statistical decay are treated. Unfortunately, dynamical models cannot account for statistical emission of fragments [29], and statistical decay models cannot include the dynamical effects that can lead to complex fragment emission before equilibrium is reached. One way around this problem is to try to include fluctuations in the dynamics [24,30,31]. Another method is to use a dynamical model to follow the early stages of the reaction, until equilibrium is reached. A statistical decay model can then be applied to follow the decay of any hot primary fragment or fragments present. In this way, a better understanding of the different processes that can lead to complex fragment emission in heavy-ion collisions at intermediate energies can be attained. These ''hybrid'' models have gained popularity in helping to interpret experimental data [32].

One of the more prevalent methods of determining the dynamical evolution of the reacting system is to solve the Landau-Vlasov (LV) [also known as the Boltzmann-Nordheim-Vlasov (BNV), Boltzmann-Uehling-Uhlenbeck (BUU), or Vlasov-Uehling-Uhlenbeck (VUU)] equation [33–38]. These models can be derived as an approximation to time-dependent Hartree-Fock calculations, and have the form

$$D_t f = \frac{df}{dt} + [f,H] = I_{\rm coll}. \tag{1}$$

This equation includes a term for the time evolution of the mean fields of the colliding nuclei, along with the collision integral $I_{\rm coll}$, which treats individual nucleon-nucleon collisions. The solution of the BNV equation can be done in a full ensemble method [38], in which a substantial number of test particles per nucleon is used to map the phase space occupa-

*Present address: Department of Physics and Astronomy, Iowa State University, Ames, IA 50011. Mailing address: Physics Department, Bldg. 510-C, Brookhaven National Laboratory, Upton, NY 11973.
†Present address: INFN - Sez. di Bari, 70126 Bari, Italy.
‡Present address: GANIL BP 5027 F14021 CAEN, France.

tion. A sufficient number of particles is required to reduce the effects that are due to numerical fluctuations caused by Monte Carlo sampling of the phase space. Since most results are quantities averaged over the entire phase space, numerical fluctuations should not cause large problems in the interpretation of the calculations [35].

In the following work, the BNV calculations are performed over a range of impact parameters, and the results are then used to parametrize inputs for the GEMINI statistical decay code [39]. In GEMINI, all possible binary decays are included, and decay chains are followed until the final nuclei no longer emit particles. The results of the GEMINI calculation are then filtered through the geometry and velocity acceptances of the detector system [40,41] to allow for comparison between the calculated and the experimental results.

II. PERFORMANCE OF THE MODEL CALCULATIONS

Performance of the dynamical model calculations by the method of Ref. [38] requires the determination of several parameters in the model: the number of test particles per nucleon, their widths in position and momentum spaces, the compressibility of the nucleus, and the nucleon-nucleon cross section. A Skyrme interaction that yields a compressibility constant of 200 MeV was used. Widths in position and momentum spaces were chosen to be 1.444 fm and 0.346 MeV/c, respectively, which reproduce the binding energies and radii of the target and projectile within 20%. Stability of the systems at nonreacting (very large) impact parameters was achieved by using 40 test particles per nucleon, and the free nucleon-nucleon cross section with its energy and angular dependence was used.[1]

The calculations were performed for the systems ^{139}La + ^{27}Al and ^{65}Cu at $E/A=45$ MeV over a range of impact parameters and time steps of 10 fm/c, up to a time of 210 fm/c. In some cases, the dynamics were followed to longer times in an attempt to verify certain features of the calculations. Once the dynamical calculations had been performed, a clusterization routine [42] was used to determine the properties of any fragment(s) present in the calculated results. These properties include the charge, mass, excitation energy, angular momentum, emission angle, and source velocity of the fragment(s). It should be noted that these calculations can account for fast-fission, deep-inelastic reactions, participant-spectator-like reactions, and (possibly) multifragmentation, and so there may be several fragments present at some, though not all, impact parameters. The clusterization routine also determines the energies and angles of particles (protons and neutrons) not included in any cluster.

In order to combine the dynamical calculations with the statistical decay model GEMINI, it is necessary to determine the time at which to end the dynamics and switch on statistical decay. In other words, at what time does the reacting system reach equilibrium? Because the dynamical model includes light-particle emission at all stages of the reaction, the determination of this time is very important. If it is too early in the reaction, then equilibrium has not been reached and GEMINI is not applicable. If it is too late, then the ''preequilibrium'' stage will also include some emission of light particles after equilibrium, and the properties of the fragment(s) will not be correctly determined for input to GEMINI. Additionally, it was assumed that shape equilibrium had been reached simultaneously with thermal equilibrium.

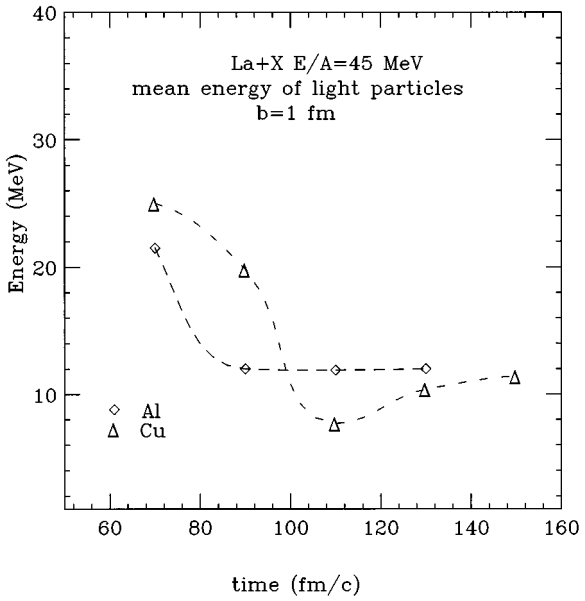

FIG. 1. Calculated mean energy of light particles emitted in the reactions ^{139}La + ^{27}Al (diamonds) and ^{nat}Cu (triangles) at an impact parameter of $b=1$ fm as a function of time. The lines are to guide the eye.

In order to determine the time at which to ''freeze-out'' the properties of the clusters and start the GEMINI calculations, the calculated mean energy of the light particles emitted was determined as a function of time. Figure 1 shows this quantity for the reactions ^{139}La + ^{27}Al and ^{65}Cu at $E/A=45$ MeV and $b=1$ fm. The lines are to guide the eye. For the reaction ^{139}La + ^{27}Al, the mean energy of the light particles decreases until about 90 fm/c, after which the energy is essentially constant. This change in the mean energy indicates the time at which preequilibrium emission of light particles ends, and is consistent with previously published results of the same system at a higher energy [25]. For the reaction ^{139}La + ^{65}Cu, the freeze-out time is longer, approximately 100–110 fm/c. This longer time may be due to the increase in the available energy for the reaction on the copper target. For larger energies, it should take more nucleon-nucleon collisions to thermalize the energy, thus more time. The fluctuations in the mean energy of the light particles at longer times in the reaction ^{139}La + ^{65}Cu are due to an oscillation in the density of the fusion residue, shown as a function of time in Fig. 2. The composite system undergoes a compression-expansion stage, with density fluctuations that eventually damp out.

[1]In the version of the BNV code used, an error in the determination of the in-medium nucleon-nucleon cross section caused an underestimation of the excitation energy of the composite system formed in the most central ($b=1$ fm) collisions. However, for larger impact parameters, identical results were obtained for both the corrected and uncorrected versions of the code. Since the bulk of the complex fragments originate from collisions with $b>1$, the results presented in Sec. III are unaffected.

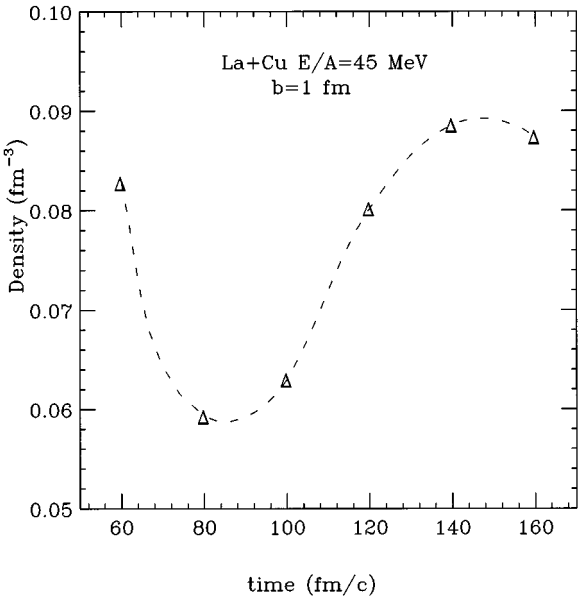

FIG. 2. Density of the composite system (in fm^{-3}) as a function of time for the reaction ^{139}La + ^{nat}Cu at $b=1$ fm. The line is to guide the eye.

III. RESULTS AND COMPARISON TO EXPERIMENTAL DATA

A. Reaction ^{139}La + ^{27}Al at E/A = 45 MeV

Contour plots of the time evolution of the density distribution of nucleons in space for the reaction ^{139}La + ^{27}Al at $E/A=45$ MeV for a range of impact parameters are shown in Fig. 3. In this figure, which is shown in the center-of-mass system, the projectile is at the left and the target is at the right at $t=0$. For the most central collisions, a hot fused system is formed. This system is highly deformed because the target and nucleus compress as they react and fuse. This distorted nuclear system will eventually reach thermal and shape equilibria and then decay statistically. At large impact parameters, the reaction is more reminiscent of deep-inelastic collisons, in which a short-lived, rotating dinuclear system

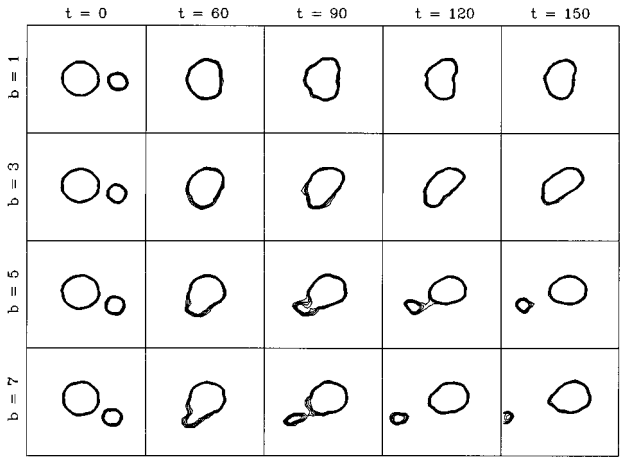

FIG. 3. Contour plots of the distribution of nucleons in space as a function of time for the reaction ^{139}La + ^{27}Al for several impact parameters. The time steps are in units of fm/c, and the impact parameters (b) are in units of fermis.

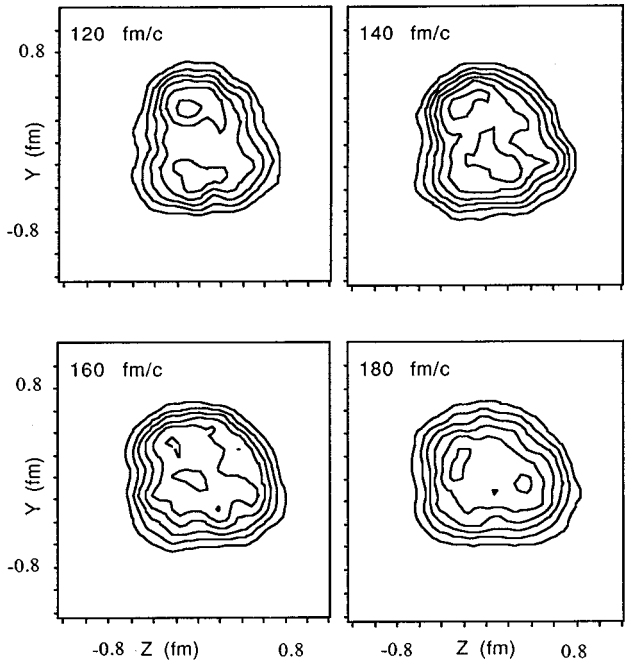

FIG. 4. Contour plots of the distribution of nucleons in space for the reaction ^{139}La + ^{27}Al at $b=3$ fm and times of 120, 140, 160, and 180 fm/c. Z is the beam direction; Y is the out-of-plane axis.

forms and then the projectilelike and targetlike fragments reseparate. There can be considerable exchange of nucleons between the target and projectile, along with excitation of the fragments, which subsequently decay by the emission of light particles. The picture is less clear for the intermediate ($b=3$ and 4 fm) impact parameters.

While at first glance the reaction at $b=3$ fm seems to be similar to the more central collisions, this may not be the case. The possibility of a fast-fission reaction mechanism [43] at these impact parameters warrants a closer look at the density distribution of nucleons in space for these reactions. An extra-push model calculation [44] indicates that for this reaction fast fission should occur at ℓ waves corresponding to an impact parameter between 2 and 3 fm. To further study the possibility of a fast-fission-like component in the dynamical calculations in this reaction, contour plots of the density of nucleons in space for various times at $b=3$ fm are shown in Fig. 4. It is clear that there are two regions of high density of nucleons for the reaction at this impact parameter on a time scale that is consistent with asymmetric fast fission for systems at similar masses and energies [43]. The two regions of high density are still present at times of up to 300 fm/c [45], but are damped out by evaporative effects at larger times.

To determine whether a fast-fission mechanism is reflected in the experimental data, the properties (charge, mass, angular momentum, and excitation energy) of the system were determined at $b=3$ and 4 fm by considering the hot source produced in the calculation to be a single hot nucleus and also by dividing in space between the two centers of density to form two hot fragments. The properties of the fragment(s) were then parametrized, including the information from the other impact parameters, and GEMINI calculations were performed.

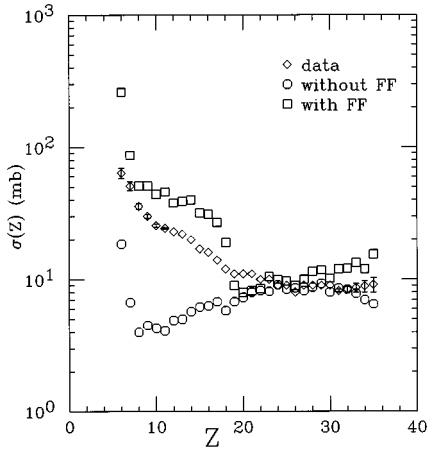

FIG. 5. Experimental (diamonds) and calculated (circles and squares) fragment cross sections for the reaction ^{139}La + ^{27}Al at $E/A=45$ MeV. The circles are for the scenario not including fast fission; the squares include fast fission. The error bars indicate the uncertainty associated with the fitting procedure of the inclusive angular distributions.

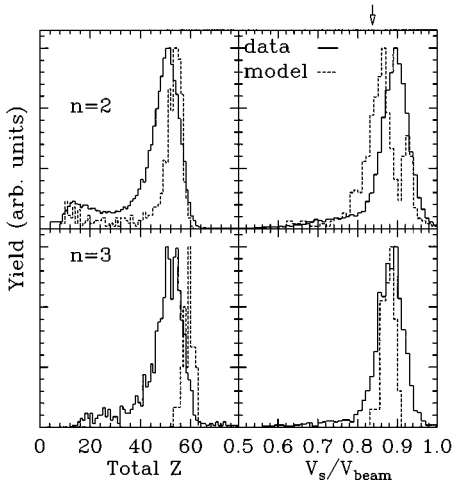

FIG. 6. Experimental (solid line) and calculated (dashed line) total detected charge and source velocity distributions for $n=2$ and 3 events for the reaction ^{139}La + ^{27}Al at $E/A=45$ MeV. The arrow is at the source velocity for complete fusion between the target and projectile.

The experimental fragment cross sections $\sigma(Z)$, and the cross sections calculated both with and without the fast-fission scenario are shown in Fig. 5. It is clear that including fast fission better reproduces the cross sections for fragments with $Z\leqslant 20$. The absolute magnitude of the distribution is reproduced by the calculations for a substantial fraction of the emitted fragments, and the general shape of the distribution is reproduced over the entire range of fragments studied. For the rest of the results concerning this reaction, the fast-fission scenario will be used. The properties of the fragments derived from the dynamical calculations and used as inputs to GEMINI for several impact parameters are shown in Table I.

Figure 6 shows the total charge and source velocity distributions for the experimental data (solid line) and the model calculations (dashed line) for events with a complex fragment multiplicity n equal to 2 and 3. The calculated distributions were filtered through the detector angular and velocity acceptances to compare to the experimental data; the arrow is at the source velocity for complete fusion. For the $n=2$ events, the peak in the total detected charge distributions $Z_{\rm tot}$ is well reproduced by the calculation, but the tail at low $Z_{\rm tot}$ is vastly underpredicted. This effect is most likely due to underestimating the contamination from $n=3$ events, because the low $Z_{\rm tot}$ tail is interpreted as due to $n=3$ events for which only two fragments were detected [7,45,52]. For $n=3$ events, the model overpredicts the charge at the peak of the distribution and underestimates both the width and the tail. Virtually no $n=4$ events were produced by the calculation. The model reproduces the peaks in the V_S distributions for both the $n=2$ and 3 events, but underestimates the tail of the distribution for the $n=3$ events. The double peak in the $n=2$ V_S distribution is due to the abrupt change in the reaction mechanism between $b=2$ and 3 fm from fusion (or incomplete fusion) to fast fission. This leads to a discontinuity in the parametrizations of the properties of the fragment(s) at the ℓ wave of the transition.

Another way of characterizing reactions in which three complex fragments are detected is to construct a Dalitz plot of the atomic numbers of the three fragments. A schematic of a charge-Dalitz plot is shown in Fig. 7. The scales in the figure run from the edges of the triangle to the opposite vertex and have a value of $Z_i/Z_{\rm tot}$, in which Z_i is the charge of the ith fragment ($i=1$, 2, or 3) and $Z_{\rm tot}$ is the total detected charge of the event. The fragments are randomized as to which is 1, 2, or 3. In addition, a minimum total detected charge of 30 is required to ensure good kinematic characterization of the event. In a charge-Dalitz plot, if the yield is concentrated at the vertices, then the event has one large and two small fragments. An event with three nearly equal-sized fragments would show up in the center of the plot. Experimental and calculated charge-Dalitz plots are shown in Fig. 8. The general trend of the experimental data, in which the charge-Dalitz plot is populated predominantly at the vertices,

TABLE I. Parameters derived from the dynamical calculation used as inputs to GEMINI for heavy and light fragments for the reaction ^{139}La + ^{27}Al as a function of impact parameter.

b (fm) Heavy	Z	A	E^* (MeV)	J ($\hbar$)	b (fm) Light	Z	A	E^* (MeV)	J ($\hbar$)
1	65	153	581	22					
3	44	102	356	27	3	20	43	73	7
5	55	129	241	55	5	8	18	77	8
7	57	133	189	50	7	8	19	68	7

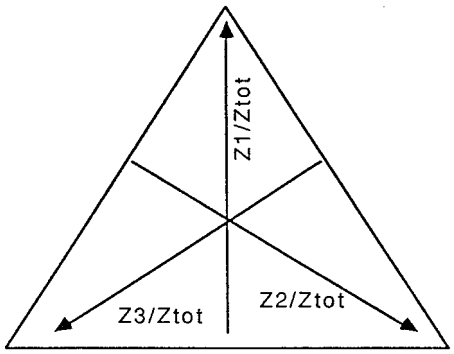

FIG. 7. Schematic diagram of a charge-Dalitz plot.

corresponding to asymmetric decays, is reproduced by the calculation. However, for the experimental data, the central region, corresponding to symmetric decays, shows some yield. On the other hand, the central region of the charge-Dalitz space for the model calculations shows a large hole or a lack of symmetric decays produced by the modeling of this reaction.

The agreement or disagreement between the experimental and calculated results can also be examined by determining the branching ratios of the multiple fragment events, shown in Table II. It is apparent that the model vastly underpredicts the amount of $n=3$ and 4 events. By comparing the results of Figs. 5 and 6 with those presented in Fig. 8 and Table II, it is apparent that the agreement between the experimental and calculated results depends on which observables are examined. While global features, such as the inclusive fragment cross sections and total charge and source velocity distributions of multiple fragment events, have been adequately described by the calculations, finer features, such as the event branching ratios, have not.

TABLE II. Experimental and calculated proportions of multiple fragment events for the reaction ^{139}La + ^{27}Al at $E/A=45$ MeV.

Multiplicity	Data	Calculation
2	0.909	0.938
3	0.086	0.042
4	0.005	0.00025

B. Reaction ^{139}La + ^{65}Cu at E/A = 45 MeV

Contour plots of the distribution of nucleons in space for the reaction ^{139}La + ^{65}Cu for a series of impact parameters are shown in Fig. 9. The evolution of the mechanism with increasing impact parameter is similar to that for the reaction ^{139}La + ^{27}Al. However, for the most central collisions ($b=1$ fm), a new mechanism may be occurring that is not seen for the more asymmetric system ^{139}La + ^{27}Al.

The density distributions of nucleons in space for this reaction at $b=1$ fm are shown in Fig. 10. At $t=60$ fm/c, the system is hot and very compressed. As the system expands (t = 100 fm/c) fluctuations in the density distribution start to form. The fluctuations may produce clusters of nucleons in space ($t=140$ fm/c), which might be the onset of a multifragmentation process. However, these clusters do not separate but condense back into a highly distorted system by $t=300$ fm/c. There is some evidence that multifragmentation can occur on a longer time scale ($\sim$300–350 fm/c after maximum compression) [46] than indicated in the present study. Thus it is unclear whether dynamical multifragmentation actually occurs for this reaction.

Figure 9 also shows that for the central collisions the highly compressed system is approaching a disklike shape. The formation of a disk of nucleons and its subsequent multifragmentation may be due to Rayleigh-Taylor-like surface instabilitites [47]. In these instabilities, multifragmentation

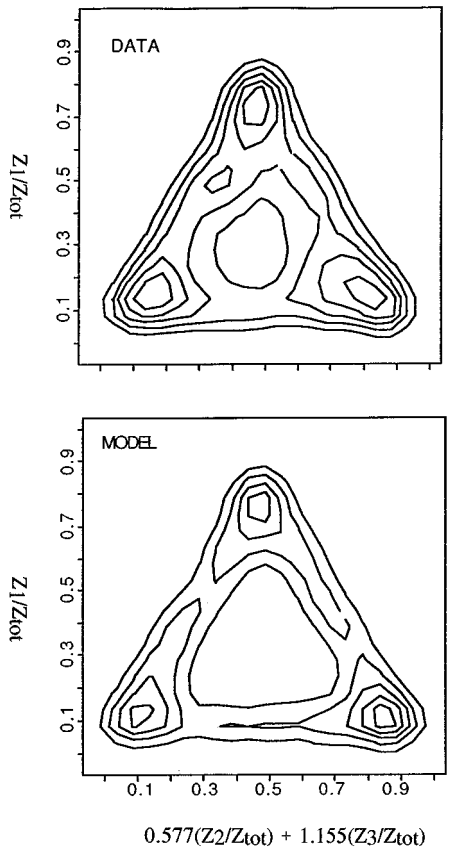

FIG. 8. Experimental (top) and calculated (bottom) charge-Dalitz plots for the reaction ^{139}La + ^{27}Al at $E/A=45$ MeV.

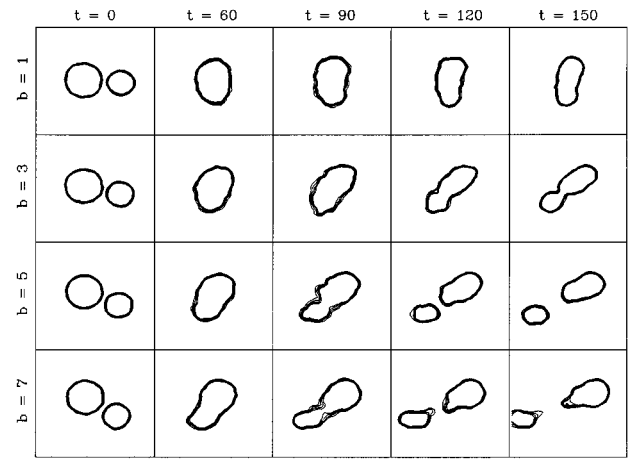

FIG. 9. Same as Fig. 3 for the reaction ^{139}La + ^{nat}Cu.

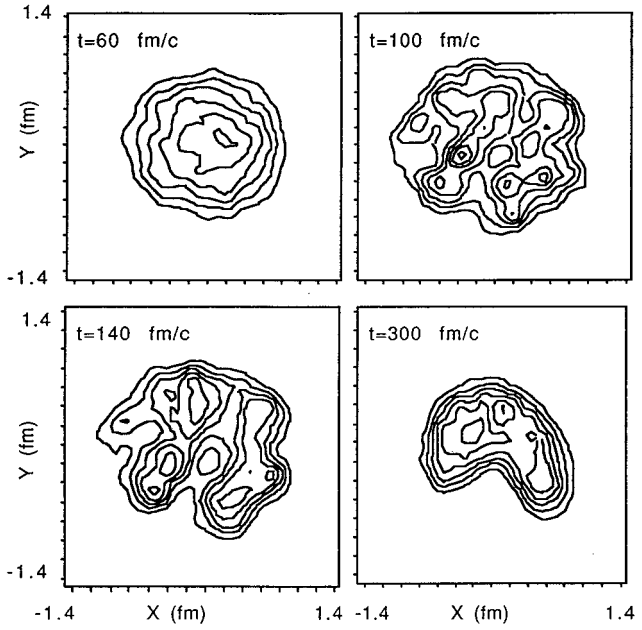

FIG. 10. Distribution of nucleons in space for the reaction ^{139}La + ^{nat}Cu at $b=1$ fm and times of 60, 100, 140, and 300 fm/c. X is the in-plane axis; Y is the out-of-plane axis.

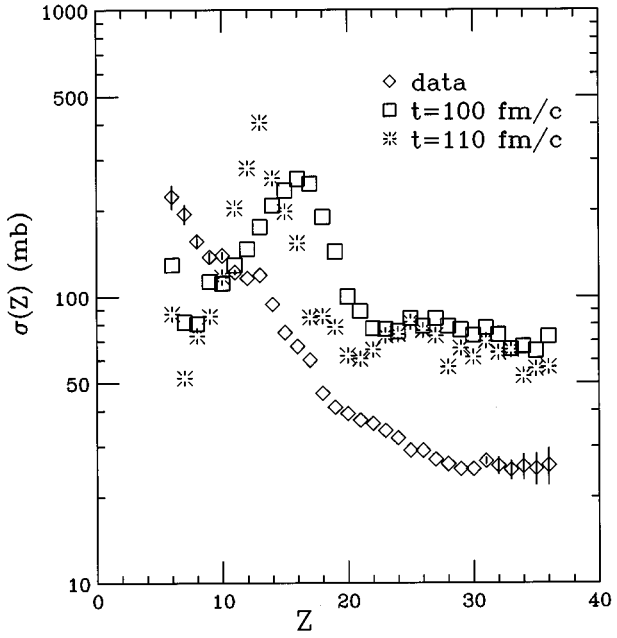

FIG. 11. Experimental (diamonds) and calculated (squares and stars) fragment cross sections for the reaction ^{139}La + ^{nat}Cu at $E/A=45$ MeV. The calculated cross sections are for two different values of the freeze-out time. The error bars are the same as in Fig. 5.

occurs because of the interactions between the two surfaces of the disk. The disk breaks into spherical fragments which have a lower total surface energy than the disk. Other dynamical model calculations for reactions of similar systems and energies show the formation of bubbles, rings, or even donuts of nucleons during the evolution of the reaction [47–50]. The formation of fragments in this reaction could also be related to spinodal decomposition of the system [51].

It is very difficult to determine the properties of the several fragments (Z, A, velocity, and angle) that may or may not have been produced in the multifragmentation scenario for the central collisions. Therefore, the central collisions were considered to proceed as in the reaction ^{139}La + ^{27}Al, in which a single hot source was formed. The properties of the fragments derived from the dynamical calculations and used as inputs to GEMINI for this reaction for several of the impact parameters studied are shown in Table III. The fragment cross sections were then determined and compared to the actual experimental cross sections, shown in Fig. 11. The calculated yield of heavy fragments is higher than the experimental yield, while the yield of lighter fragments is lower. A multifragmentation scenario in the model, whether in the dynamics or in the statistical decay portion of the calculation, would cause a decrease in the cross section of the heaviest fragments and an increase in the cross section of the lighter products. The peak in the calculated cross section distribution can be attributed to the fission of the hot nuclear system that was formed in the central collision. However, it is not possible to adequately treat the multifragmentation scenario by this model. The disagreement between the calculated and experimental fragment cross sections in the reaction ^{139}La + ^{65}Cu is in contrast to the results obtained for the reaction ^{139}La + ^{27}Al, in which both the magnitude and the shape of the fragment cross section distribution were adequately described. This change in the results shows the evolution of possible mechanisms for the emission of complex fragments as the reacting system becomes more symmetric and heavier, and as the available energy increases.

To obtain a better understanding of where the calculations may be failing for the heavier target, the total detected charge and source velocity distributions of multiple fragment events were determined, and then compared to the experimental data after filtering through the detector acceptance, as shown in Fig. 12. Surprisingly, the source velocity distributions for the $n=2$ and 3 events are fairly well reproduced by the calculation. This is very similar to the results of the cal-

TABLE III. Parameters derived from the dynamical calculation used as inputs to GEMINI for heavy and light fragments for the reaction ^{139}La + ^{65}Cu as a function of impact parameter.

b (fm) Heavy	Z	A	E^* (MeV)	J ($\hbar$)	b (fm) Light	Z	A	E^* (MeV)	J ($\hbar$)
1	67	153	811	42					
3	61	138	632	73	3	8	14	50	2
5	54	120	413	74	5	15	32	117	10
7	53	118	151	45	7	22	46	125	20

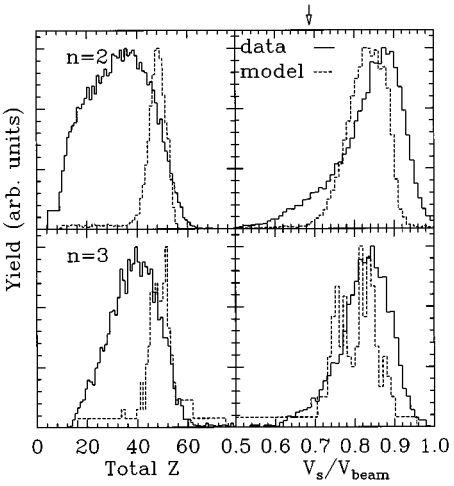

FIG. 12. Same as Fig. 6 for the reaction ^{139}La + ^{nat}Cu at $E/A=45$ MeV.

culation for the reaction ^{139}La + ^{27}Al. In an incomplete fusion model of inverse kinematics reactions, the source velocity is a function of the degree of fusion between the target and projectile and is thus an experimental observable dependent on reaction dynamics. One can then derive the source mass from the source velocity. In this case, the experimental source mass is between 150 and 170 u. This source size closely matches the total source masses (heavy plus light) shown in Table III. This agreement between the experimental and calculated source velocity distributions shows that the earliest stages of the reaction are effectively treated by the dynamical calculation. On the other hand, neither the peaks nor the tails of the Z_{tot} distribution are reproduced by the calculation. For the $n=2$ events, the experimental distribution is peaked at a much lower value than the calculation. Recalling that the modeling of this reaction did not use a possible multifragmentation scenario that may be occurring for central collisions, the lack of agreement between the calculation and the experiment could be interpreted as evidence that some type of multifragmentation is occurring for this reaction. The mechanism of this multifragmentation process is an important question that has not been answered by these calculations.

IV. DISCUSSION

The experimental results shown in this paper have been previously presented in the context of the systematics of ^{139}La-induced reactions at intermediate energies [7,45,52]. In these reactions there is an indication of statistical decay of highly excited nuclei, shown by the dependence of the multiple fragment event branching ratios on the inferred excitation energy per nucleon of the decaying system, and not on the projectile-target combination or the bombarding energy [7,45,52]. Statistical descriptions of chemical reactions often follow an Arrhenius rate law, in which the rate is proportional to $\exp(1/T)$, where T is the temperature. In nuclear matter, T is proportional to $E^{*1/2}$, and the rate can be considered the probability of multiple fragment emission. Thus, the statistical nature of the emission of three fragments may be demonstrated if a plot of the natural logarithm of the ratio

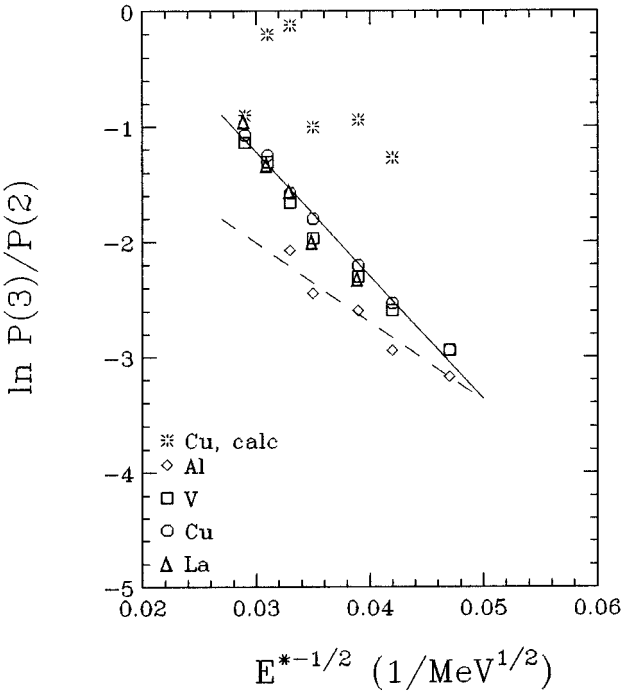

FIG. 13. Natural logarithm of the ratio $P(3)/P(2)$ as a function of $1/E^{*1/2}$ for the reactions ^{139}La + ^{27}Al, ^{51}V, ^{nat}Cu, and ^{139}La at $E/A=45$ MeV and for the results calculated in this paper. The lines are least-squares fits to the data.

$P(3)/P(2)$ as a function of $1/\sqrt{E^*}$ is linear [53,54], with $P(3)$ the probability of decay into three fragments and $P(2)$ the probability of decay into two fragments. Such a plot is shown in Fig. 13 for the experimental data from the reactions ^{139}La + ^{27}Al, ^{51}V, ^{nat}Cu, and ^{139}La at $E/A=45$ MeV [7,45,52], and also for the reaction ^{139}La + ^{65}Cu modeled in this paper. These yields have not been corrected for efficiency as was done in Ref. [53]. However, the main result of the efficiency correction was to change the magnitudes of the ratios, not the general trend of the data [53].

The behavior of the data in Fig. 13 is similar to that of Fig. 3 in Ref. [53]. The lines in Fig. 13 are the results of linear least-squares fits to the data. The data in Fig. 13 are linear over excitation energies ranging from about 3 to 7 MeV/nucleon, with the fit to the data from the reaction ^{139}La + ^{27}Al (dashed line) having a shallower slope than the fit to the data from the other reactions. It is also possible to fit the data for the heavier targets to two linear functions instead of one, with the cusp at an excitation energy of about 5 MeV/nucleon, shown in Fig. 14. The function used to fit the lower excitation energies has a similar slope to the reaction on the ^{27}Al target over the same range of excitation energy, while the line used to fit the higher excitation energies has a steeper slope. Because the slope is related to the ''potential energy'' of the system at freeze-out [53], this change in slope at an excitation energy of 5 MeV/nucleon could be an indication of a change in the decay mechanism of the heavier systems at higher excitation energies. There is some indication of similar behavior for the ^{27}Al target, but data at higher excitation energies are lacking. The difference in the results between the ^{27}Al target and the heavier targets is most likely due to the lack of an efficiency correction to

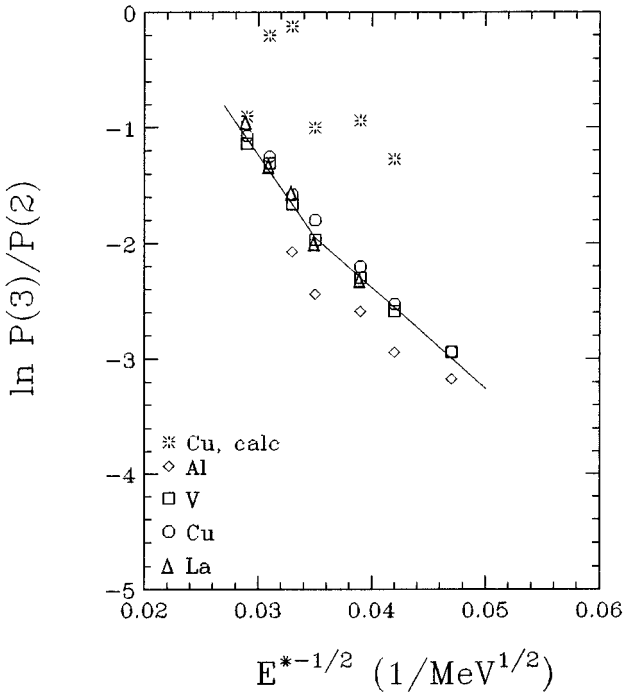

FIG. 14. Same as Fig. 13, except using two separate least-squares fits to the data for the heavier targets.

the data presented in Figs. 13 and 14. The lack of agreement between the experimental and calculated data for the reaction ^{139}La + Cu is another indication that the breakup of the composite system is not properly treated in the model used.

The use of a hybrid dynamical-statistical calculation to help interpret experimental data from other systems has met with varying degrees of success. This approach seems to work best in studying the reactions of very asymmetric systems, such as the reaction ^{139}La + ^{27}Al at $E/A=45$ MeV in this paper and at $E/A=55$ MeV [25,26]. These reactions have been shown to proceed by an incomplete fusion mechanism [7,45,52], with a source velocity between that of the projectile and the complete fusion product. For these reactions, the available energy in the center of mass is still fairly low, on the order of 3–5 MeV/nucleon (depending on the degree of fusion) and the emitting source can be well characterized in terms of source velocity and total charge [7,45,52]. The study of the reaction ^{139}La + ^{27}Al at $E/A=55$ MeV [25,26] reached similar results to those presented in this paper. The hybrid calculation reproduces experimental features such as the inclusive fragment cross sections and the total charge and source velocity distributions of multiple fragment events.

As the reacting system becomes more symmetric, the available energy increases, and the hybrid approach of dynamics plus sequential binary decay may no longer be applicable. Results similar to those presented in Fig. 10 were also exhibited in the study of the reactions ^{139}La + ^{63}Cu at E/A = 55 MeV [26] and ^{131}Xe + ^{65}Cu at $E/A=45$ MeV [27,28]. There is some agreement between the calculated results of the reaction ^{139}La + ^{65}Cu at $E/A=45$ MeV presented in this paper and the reaction ^{131}Xe + ^{65}Cu at $E/A=45$ MeV [27,28]. Differences in the experimental results arise from differences in the detector system thresholds and angular coverages for the two studies. In the lanthanum-induced reaction, the detector system covered angles close to the grazing angle (1.7°), and so the heaviest fragments were easily detected [45]. Thus, the predominant decay channel detected for the $n=3$ events was to one heavy and two light fragments [45]. However, the latter experiment did not detect fragments emitted at laboratory angles less than 5.5° [27,28]. In reverse kinematics reactions, the heavy fragments are emitted at small laboratory angles. By not including fragments emitted at small laboratory angles, the asymmetric decay channels have been suppressed, leaving only the more symmetric decays.

In the comparison between experimental and calculated results in the Xe-induced reaction, similar results to those presented in this paper were shown. These results included a failure to reproduce the magnitudes of the inclusive fragment cross sections and the total charge distributions for the $n=3$ events. However, the general shape of the fragment cross sections was reproduced. By using a statistical multifragmentation calculation linked to the dynamical one, better agreement between the experimental and calculated results was achieved [28].

While the reaction ^{139}La + ^{27}Al can be fairly well understood by the application of this hybrid calculation, the situation is less clear for the study of the reaction ^{139}La + ^{65}Cu. The hot composite system that is formed in central collisions is highly nonspherical (and possibly fragmented due to dynamical instabilities) and undergoes density oscillations well past the time when thermal equilibrium is reached. The use of GEMINI is only prescribed for spherical nuclei near equilibrium density [39]. While these conditions may have been met in the study of the reaction ^{139}La + ^{27}Al, it is clear from Figs. 2, 9, and 10 that they have not been met for the reaction ^{139}La + ^{65}Cu. By showing that the source velocity distribution, which can infer a source size, for the multiple fragment events in the lanthanum-induced reaction is adequately reproduced by the dynamical calculation, this paper has explicitly shown that the early stages of the reaction are well characterized by the dynamical calculation. It is only at the fragment emission stage that this calculation fails to reproduce the results sensitive to the mechanism of fragment emission.

V. SUMMARY

The results of Figs. 13 and 14, Refs. [7,45,52] suggest that complex fragment emission is dominated by statistics, but provides no evidence on whether the process is sequential or prompt. To further investigate the relative roles of dynamics and statistics a hybrid model consisting of a first stage that describes the dynamics of the collision and second stage that describes the sequential decay of the primary product(s) was utilized. This approach works best for systems that are still at faily low excitation energy, but fails when the excitation energy increases. The present study shows the importance of determining the source velocity distribution of the multiple fragment events in the study of complex fragment emission at intermediate energies. For the reaction ^{139}La + ^{65}Cu at $E/A=45$ MeV, for which there is not a match between fragment cross sections or total charge distributions determined experimentally and by the model, there is

good agreement in the source velocity distributions. In the geometric incomplete fusion model, the source velocity is a measure of the degree of fusion between the target and projectile. In other words, the source velocity is a variable sensitive to the reaction dynamics. The agreement between the experimental data and the calculated data in the determination of the source velocity for this reaction shows that the failure in the reproduction of the other experimental observables, such as the fragment cross sections, is due to a poor description of the fragment emission stage, whether due to a dynamical disassembly of a highly excited source or to limitations of the sequential binary decay calculation.

ACKNOWLEDGMENT

This work was supported by the U.S. Department of Energy under Grant No. DEFG05-87-ER40321.

[1] D.R. Bowman *et al.*, Nucl. Phys. **A523**, 386 (1991).
[2] D.R. Bowman *et al.*, Phys. Rev. C **46**, 1834 (1992).
[3] R. Bougault, J. Colin, F. Delauney, A. Genoux-Lubain, A. Hafjani, C. LeBrun, J.F. Lecolley, and J. Steckmeyer, Phys. Lett. B **232**, 3 (1989).
[4] R. Bougault *et al.*, Nucl. Phys. **A488**, 255c (1988).
[5] K. Hagel *et al.*, Phys. Rev. Lett. **68**, 2141 (1992).
[6] B. Lott *et al.*, Phys. Rev. Lett. **68**, 3141 (1992).
[7] P. Roussel-Chomaz *et al.*, Nucl. Phys. **A551**, 508 (1993).
[8] S. Yenello *et al.*, Phys. Rev. Lett. **67**, 671 (1991).
[9] D. Fox *et al.*, Phys. Rev. C **47**, R421 (1993).
[10] T.C. Sangster, M. Begemann-Blaich, Th. Blaich, H.C. Britt, A. Elmaani, N.N. Ajitanand, and M.N. Namboodiri, Phys. Rev. C **47**, R2457 (1993).
[11] D.E. Fields, K. Kwiatkowski, K. B. Morley, E. Renshaw, J.L. Wile, S.J. Yennello, V.E. Viola, and R.G. Korteling, Phys. Rev. Lett. **69**, 3713 (1992).
[12] M.B. Tsang *et al.*, Phys. Rev. Lett. **71**, 1502 (1993).
[13] E. Bauge *et al.*, Phys. Rev. Lett. **70**, 3705 (1993).
[14] D.R. Bowman *et al.*, Phys. Rev. Lett. **70**, 3534 (1993).
[15] T. Li *et al.*, Phys. Rev. Lett. **70**, 1924 (1993).
[16] R.A. Lacey *et al.*, Phys. Rev. Lett. **70**, 1224 (1993).
[17] S.R. Souza, L. dePaula, S. Leray, J. Nemeth, C. Ngo, and H. Ngo, Nucl. Phys. **A571**, 159 (1994).
[18] V. Latora, A. Del Zeppo, and A. Bonasera, Nucl. Phys. **A572**, 477 (1994).
[19] W.A. Friedman, Phys. Rev. C **42**, 667 (1990).
[20] D.H.E. Gross, Phys. Lett. B **203**, 26 (1988).
[21] J.P. Bondorf, R. Donangelo, I.N. Mishutin, and H. Schulz, Nucl. Phys. **A444**, 460 (1985).
[22] J.A. Lopez and J. Randrup, Nucl. Phys. **A503**, 183 (1989).
[23] J.A. Lopez and J. Randrup, Nucl. Phys. **A512**, 345 (1990).
[24] J. Randrup, Nucl. Phys. **A574**, 133c (1994).
[25] M. Colonna *et al.*, Phys. Lett. B **283**, 180 (1992).
[26] M. Colonna, N. Colonna, A. Bonasera, and M. DiToro, Nucl. Phys. **A541**, 295 (1992).
[27] M. Bruno *et al.*, Phys. Lett. B **292**, 251 (1992).
[28] M. Bruno *et al.*, Nucl. Phys. **A576**, 138 (1994).
[29] A. Adorno, A. Bonasera, M. Cavinato, M. Colonna, A. Cunsolo, G.C. DiLeo, M. DiToro, and F. Gulminelli, Nucl. Phys. **A529**, 565 (1991).
[30] P. Chomaz, G.F. Burgio, and J. Randrup, Phys. Lett. B **254**, 340 (1990).
[31] G.F. Burgio, Ph. Chomaz, and J. Randrup, Nucl. Phys. **A529**, 157 (1991).
[32] L.G. Moretto and G.J. Wozniak, Annu. Rev. Nucl. Part. Sci. **43**, 379 (1993).
[33] G.F. Bertsch and S. Das Gupta, Phys. Rep. **160**, 189 (1988), and references therein.
[34] C. Gregoire, C. Ngo, and B. Remaud, Nucl. Phys. **A383**, 393 (1982).
[35] C. Gregoire, B. Remaud, F. Sebille, L. Vinet, and Y. Raffray, Nucl. Phys. **A436**, 365 (1985).
[36] B. Remaud, F. Sebille, C. Gregoire, L. Vinet, and Y. Raffray, Nucl. Phys. **A447**, 555c (1985).
[37] B. Remaud, F. Sebille, C. Gregoire, and L. Vinet, Nucl. Phys. **A488**, 423c (1985).
[38] A. Bonasera, G.F. Burgio, and M. DiToro, Phys. Lett. B **221**, 233 (1989).
[39] R.J. Charity, D.R. Bowman, Z.H. Liu, R.J. McDonald, M.A. McMahan, G.J. Wozniak, L.G. Moretto, S. Bradley, W.L. Kehoe, and A.C. Mignerey, Nucl. Phys. **A476**, 516 (1988).
[40] W.L. Kehoe *et al.*, Nucl. Instrum. Methods Phys. Res. A **311**, 258 (1992).
[41] J.T. Walton, H.A. Sommer, G.J. Wozniak, G.F. Peaslee, D.R. Bowman, W.L. Kehoe, and A. Moroni, IEEE Trans. Nucl. Sci. **NS-37**, 1578 (1990).
[42] A. Bonasera, M. Colonna, M. DiToro, F. Gulminelli, and H.H. Wolter, Phys. Lett. B **244**, 169 (1990).
[43] D.J. Hinde, D. Hilscher, and H. Rossner, Nucl. Phys. **A502**, 497c (1989).
[44] W.J. Swiatecki, Nucl. Phys. **A376**, 275 (1982).
[45] B. Libby, Ph.D. thesis, University of Maryland, 1992.
[46] D. Durand *et al.*, Phys. Lett. B **345**, 397 (1995).
[47] L.G. Moretto, K. Tso, N. Colonna, and G.J. Wozniak, Phys. Rev. Lett. **69**, 1884 (1992).
[48] W. Bauer, G.F. Bertsch, and H. Schulz, Phys. Rev. Lett. **69**, 1888 (1992).
[49] H.M. Xu, C.A. Gagliardi, R.E. Tribble, and C.Y. Wong, Nucl. Phys. **A569**, 575 (1994).
[50] D.H.E. Gross, B-A. Li, and A.R. DeAngelis, Ann. Phys. (Leipzig) **1**, 467 (1992).
[51] E. Suraud, M. Pi, P. Schuck, B. Remaud, F. Sebille, C. Gregoire, and F. Saint-Laurent, Phys. Lett. B **229**, 359 (1989).
[52] Y. Blumenfeld *et al.*, Phys. Rev. Lett. **66**, 576 (1991).
[53] L.G. Moretto, D.N. Delis, and G.J. Wozniak, Phys. Rev. Lett. **71**, 3935 (1993).
[54] J. Pouliot, L. Beaulieu, B. Djerroud, D. Dore, R. Laforest, R. Roy, C. St-Pierre, and J.A. Lopez, Phys. Rev. C **48**, 2514 (1993).